Topology Finding of Structural Patterns

Robin Oval, Matthias Rippmann, Romain Mesnil, Tom van Mele, Olivier Baverel, Philippe Block

AAG2018

Advances in Architectural Geometry 2018
Chalmers University of Technology
Gothenburg, Sweden
22-25 September 2018

www.architecturalgeometry.org/aag18

Topology Finding of Structural Patterns

Robin Oval[1,2], Matthias Rippmann[2], Romain Mesnil[1], Tom Van Mele[2], Olivier Baverel[1], Philippe Block[2]

[1] Navier, UMR 8205, École des Ponts, IFSTTAR, CNRS, UPE, Champs-sur-Marne, France
robin.oval@enpc.fr
olivier.baverel@enpc.fr
romain.mesnil@enpc.fr

[2] ETH, Institute of Technology in Architecture, Block Research Group, Zürich, Switzerland
oval@arch.ethz.ch
rippmann@arch.ethz.ch
van.mele@arch.ethz.ch
block@arch.ethz.ch

Abstract

This paper presents a strategy for topological exploration of structural patterns, such as beam grids for gridshells or voussoir tessellations for masonry vaults. The authors define *topology finding*, by analogy and in complement to form finding, as the design of the connectivity of patterns in relation to architectural and structural requirements. The method focuses on the design of the singularities in the pattern through the automated generation and subsequent rule-based editing of a coarse quad mesh that encodes the properties of the singularities and their relationships before mesh densification, pattern mapping, geometrical exploration and performance assessment.

Key words: structural design, structural morphology, discrete shells, structural patterns, topology, topological exploration, topology finding

1 Introduction

1.1 Structural patterns

Shell structures span large areas efficiently thanks to their double curvature that provides geometrical stiffness. These structures are often discretised in a pattern, which constitutes the load-bearing system once fabricated and assembled. Beam grids for gridshells or voussoir tessellations for masonry vaults are such examples of structural patterns for shells (Figure 1). The design of structural patterns is a complex and rich process influenced by many aspects of the projects, such as aesthetics, statics, fabrication, assembly, as well as sustainability and cost.

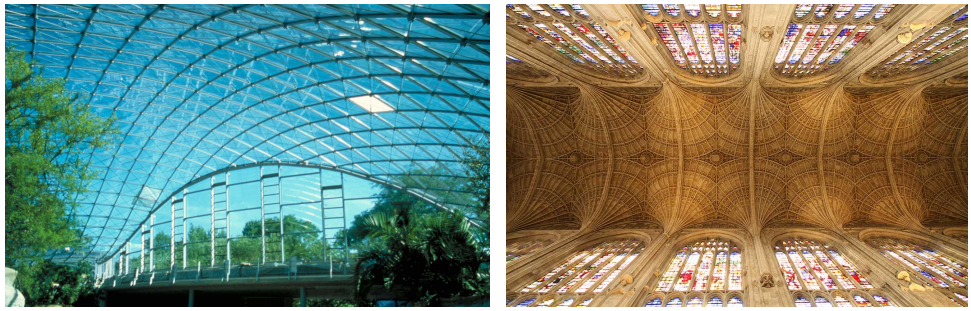

(a) (b)

*Figure 1: Two examples of structural patterns for shell-like structures: (**a**) beam grid of the Hippo House in Berlin, Germany (photo credit: sbp.de) and (**b**) voussoir tessellation of the King's College Chapel in Cambridge, England (photo credit: kings.cam.ac.uk).*

1.2 Topology of patterns

Reciprocally, the choice of pattern greatly influences these criteria since a pattern performs better for some criteria and worse for others. More specifically, the topology – or connectivity – of a structural pattern matters because it sets the bounds of the geometrical design space, within the general design space, for form finding and other geometrical design approaches. This geometrical design space, which represents all the possible geometries for a given topology, may not contain efficient or even feasible designs. Indeed, the topology, and more specifically the set of singularities in a pattern, define the qualitative degrees of freedom for design and optimisation, as illustrated by Schiftner and Balzer (2010) for competing statics and fabrication requirements. For this reason, designers need conceptual and practical tools to allow them to flexibly and efficiently explore the topology of structural patterns during early-stage design, as stated by Harding et al. (2012), and make design choices which balance the different performance requirements.

1.3 Contributions and outline

This research introduces *topology finding* of structural patterns. Topology finding deepens the available design space for geometrical exploration. The authors use a specific design space structure and focus on the design of the singularities through a coarse quad mesh.

This new practical design tool is implemented as a package for COMPAS (Mele et al. (2017)), an open-source computational Python framework for researchers, professionals and students working in the fields of architecture, engineering and digital fabrication.

Section 2 shows the design space structure used for topological design of patterns. Section 3 develops an automated generation scheme for the singularities of the pattern using the medial axis of a shape. Section 4 presents a rule-based editing method for the singularities of the pattern using a grammar. Section 5 illustrates how to visualise designs from a topological space based on their relative performance.

2 Design spaces

Topology finding relates to the exploration of the three topology-related design spaces: singularities, density and pattern, in complement to the geometrical design space. These design spaces derive from each other as shown in Figure 2 for the gridshell of the Great Court at the British Museum in London, England, whose geometry has been analytically defined by Williams (2001), and which serves as main example throughout this paper.

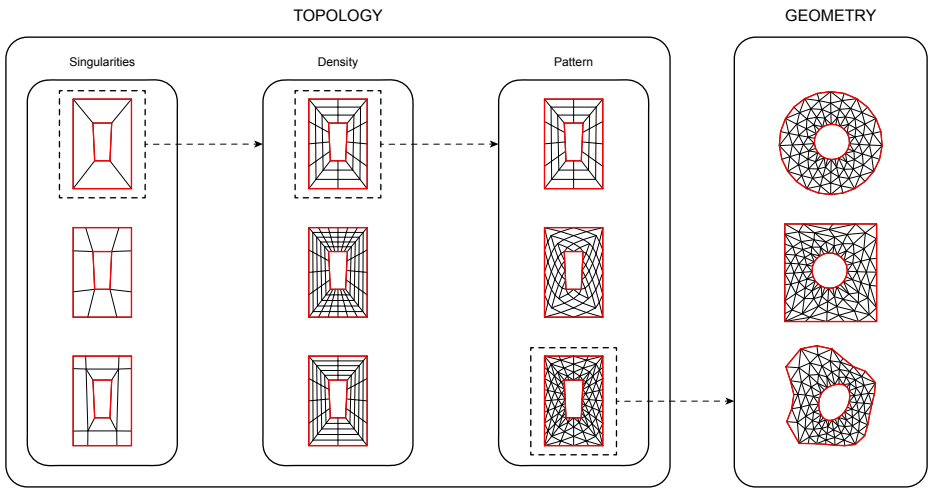

Figure 2: The design space structure for topological exploration of patterns.

The design of the singularities in a pattern is handled at the level of a coarse quad mesh (which can also be referred to as control mesh or patch set), which includes the vertices which represent the singularities and whose edges represent their connectivity in the pattern, and which defines the parameterisation directions of the shape.
The density is set through densification of the coarse quad mesh into a quad mesh and the pattern is derived from a transformation of the quad mesh elements, for instance through global conversion of the initial quad mesh into its dual mesh, its diagonal mesh or through triangulation, supplemented by local modifications.
The geometry of the pattern is explored through smoothing, form finding, form optimisation etc. Although presented linearly, the designer can move downstream and upstream the design space structure during the design process.

All the patterns that are presented in this paper are untrimmed and characterised as being aligned with the boundaries, which benefits the aesthetics, favors loads paths parallelly or perpendicularly to the boundaries and avoids the creation of irregular elements to fabricate and assemble. However, this characteristic can induce practical limitations when performing planarisation with constrained straight boundaries, as mentioned by Tang et al. (2014).

The first challenge is about how to enter the design space, manual drawing of a coarse quad mesh requiring time and experience.

3 Automated generation

We describe a scheme to automatically generate an initial coarse quad mesh, and a corresponding pattern, on a NURBS surface input. The input surface is initially mapped to the plane based on its UV-parameterisation, then the coarse quad mesh is generated on the planar map before being remapped back onto the surface. The density and the pattern are set, before being relaxed on the surface and further processed.

3.1 Singularities

The singularities are derived from the medial axis of the surface, also known as its topological skeleton, introduced by Blum (1967), which consists in a dimensional reduction of the the surface into a set of curves called medial branches. The steps of the process to obtain a coarse quad mesh are show in Figure 3.

The input NURBS surface is mapped to the plan and its boundaries are subdivided into a set of vertices for a Delaunay triangulation. The key points from the Delaunay mesh are: the singular points S at the centroids of singular faces (faces adjacent to three other faces), the boundary points B at the vertices of singular faces, and the corner points C (two-valent boundary vertices). The medial axis is

constituted by the branches connecting the circumcentres of the adjacent Delaunay faces: the S-S and S-C branches. The medial axis defines a natural decomposition of the surface with singularities stemming from its topology. Three simple heuristics based on the connectivity of the Delaunay mesh, which relate to Rigby (2003), are used to generate a coarse quad mesh from the medial axis: pruning to remove the S-C branches; grafting to add the S-B branches; and closing to add the B-B and B-C branches. The extracted connectivity of these branches defines the coarse quad mesh.

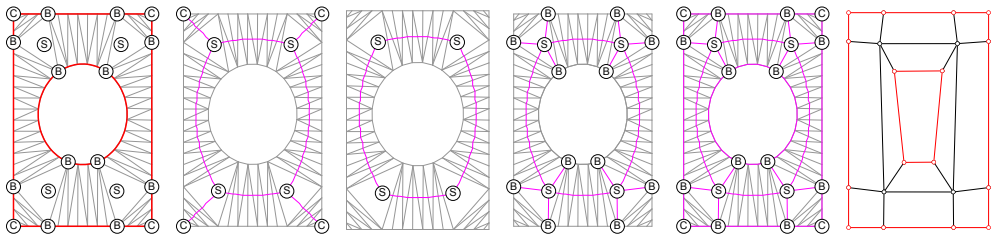

*Figure 3: Medial-axis-based automated generation of a coarse quad mesh from the planar map of an input surface: (**a**) triangulation, (**b**) skeletonisation, (**c**) pruning, (**d**) grafting, (**e**) closing, (**f**) extraction.*

3.2 Pattern

From the automatically generated coarse quad mesh, a smooth pattern can be directly generated on the input surface, as shown in Figure 4. Once the singularities are generated and the coarse quad mesh is mapped back onto the input surface, the density and the pattern can be chosen.

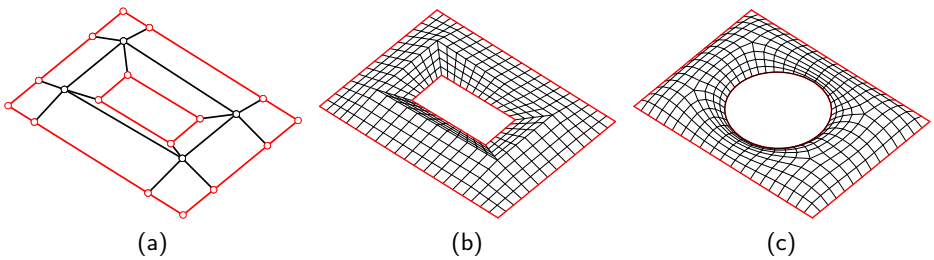

*Figure 4: Automated generation of a smooth quad mesh on a surface from a coarse quad mesh: (**a**) remapping, (**b**) densification, (**c**) relaxation.*

The density of the pattern is controlled per quad face strip in the coarse quad mesh, because each pair of opposite edges in each quad face share the same density parameter. The dependent edges are grouped in independent groups that correspond to the density parameters per face strip. The designer controls all of these degrees of freedom and can automatically compute subdivision parameters based on a target

length and the average length of the edges in each group. The coarse quad mesh is then densified into a quad mesh that sets the density of the pattern.

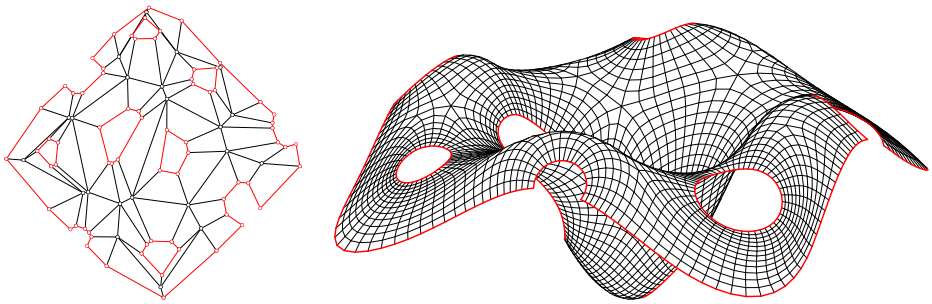

(a) (b)

*Figure 5: Automated generation of a smooth quad mesh on an input free-form surface: (**a**) coarse quad mesh, (**b**) smooth quad mesh.*

The pattern is relaxed on the surface with constraints at boundary corners and along boundary curves using a smoothing algorithm, such as (area-weighted) Laplacian smoothing (Botsch et al. (2010)), to provide a smooth starting geometry for further exploration. Figure 5 shows an example with stronger double curvature after automated generation of a coarse quad mesh and tuned densification and relaxation, necessary to compensate the distortions between the coarse quad mesh and the NURBS surface, even though the vertices of the mesh lie on the surface.

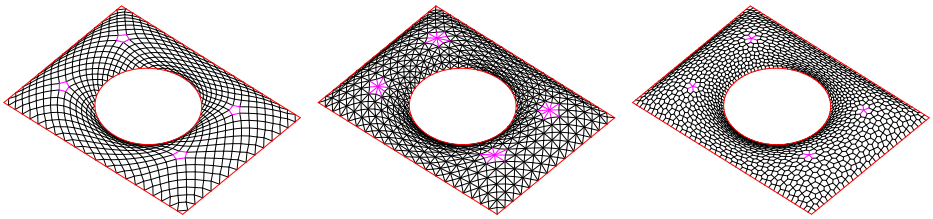

(a) (b) (c)

*Figure 6: Automated generation of smooth patterns on a surface using Conway operators: (**a**) ambo, (**b**) kis, (**c**) gyro, with singular elements highlighted in magenta.*

The pattern is derived from global transformation of the quad mesh and its elements, for instance using the operators by Conway et al. (2016), as shown in Figure 6 applied to the quad mesh in Figure 4, and already investigated by Shepherd and Pearson (2013) adn applied to the original pattern of the British Museum. The singularities from the quad mesh are converted into irregular vertices or faces in the pattern. Another round of constrained relaxation on the surface provides smoothness to the pattern.

3.3 Form finding

The input surface provides a starting geometry with the main topological information. Figure 7 shows a thrust network resulting from a funicular form finding process using RhinoVAULT (Rippmann and Block (2013)) after conversion of the relaxed pattern into a form diagram projected to the XY plane. The input curved surface serves as design intent and helps to reduce the element distortion due to the slope.

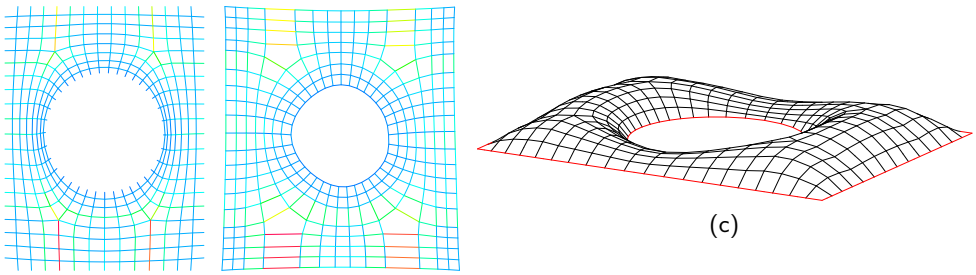

*Figure 7: Funicular form finding revisiting the geometry of the British Museum: (**a**) form diagram, (**b**) force diagram (rotated by 90°), (**c**) thrust network.*

Nevertheless, a planar input surface is sufficient to generate a pattern, as shown for the design in Figure 8, inspired by the Solemar baths in Bad Dürrheim, Germany. The quad mesh structure, the smoothness, the low number of singularities and the alignment to the boundaries permit clear readability between the reciprocal form and force diagrams, a key aspect of interactive graphical design methods and empowers the designer to perform force-based geometrical exploration.

3.4 Pole points

Pole points are a special type of singularities whose valency depends on the density of the pattern. Poles are integrated in the coarse quad mesh by allowing pseudo-quad faces which are geometrically as triangles but topologically as quads with a double vertex at the pole location, as shown in Figure 9.

Point features complete the input data. These points are added to the set of vertices of the Delaunay mesh, which displays thereby additional singular faces around the point features. The resulting coarse quad mesh includes pseudo-quad faces around the point features, which serve as double vertices, marked as filled dots. Thus, the generated pattern features additional singularities and poles.

Poles can stem from statics reasons such as concentrated forces, loads or reactions, or geometrical reasons such as umbilical points.
The design in Figure 10 revisits the ribbed slabs of Pier Luigi Nervi by showing a smooth planar quad mesh with multiple point features: although the pattern does not derive from the integration of principal stress directions for a load combination,

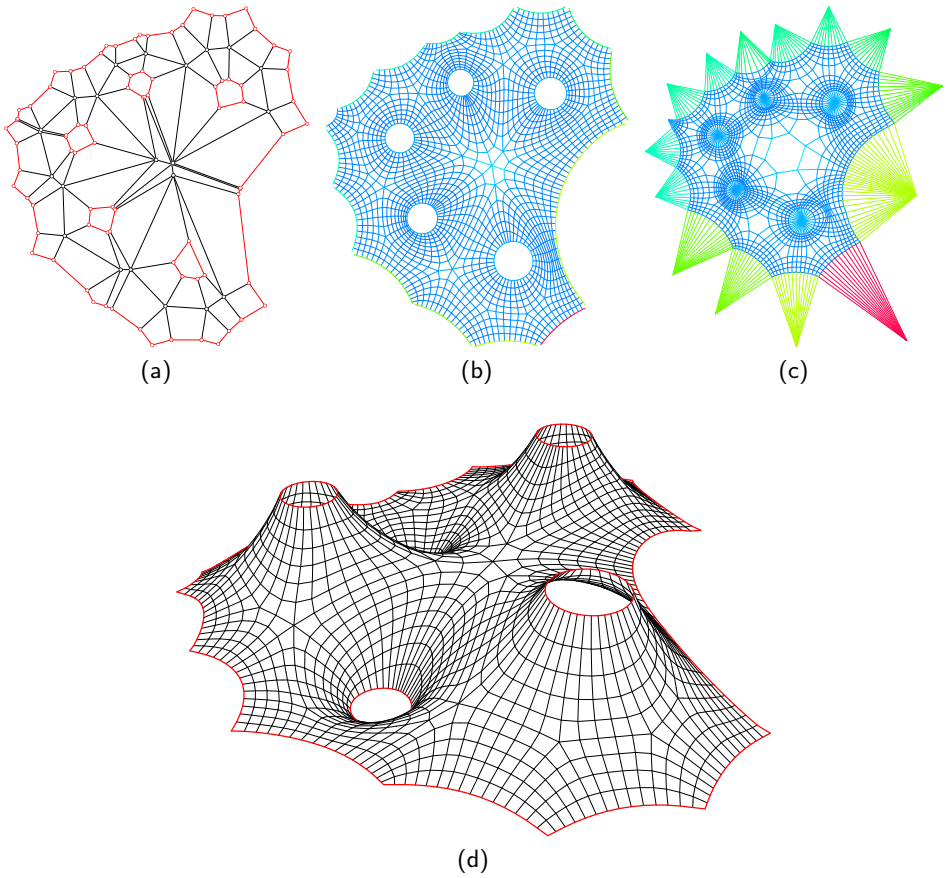

*Figure 8: Automated topological generation and funicular form finding revisiting the Solemar baths in Bad Dürrheim, Germany: (**a**) coarse quad mesh, (**b**) form diagram, (**c**) force diagram (rotated by 90°), (**d**) thrust network.*

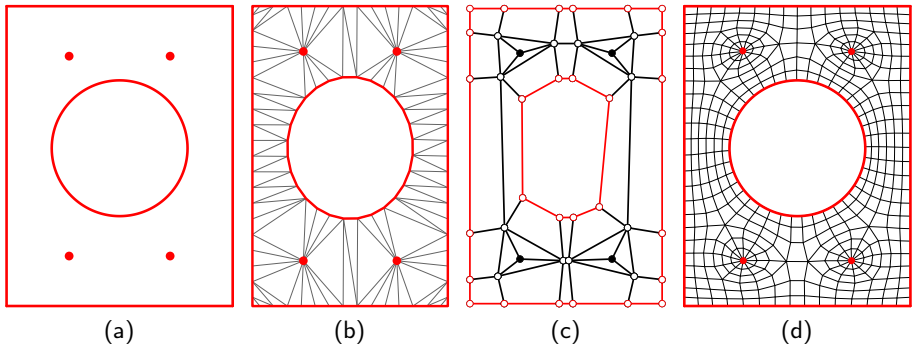

*Figure 9: Automated generation of a smooth quad mesh with poles: (**a**) input with point features, (**b**) Delaunay mesh, (**c**) coarse quad mesh, (**d**) smooth quad mesh with poles.*

the design is informed by the statics system by heuristically adding poles at the location of columns to provide a high number of load paths towards the supports.

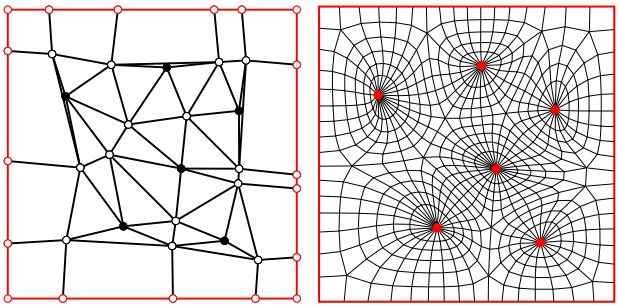

*Figure 10: Automated generation of a smooth quad mesh with multiple poles: (**a**) coarse quad mesh with pseudo-quad faces, (**b**) smooth quad mesh with poles.*

The second challenge is about how to move in the design space, since the singularities from the medial axis may not be the best choice regarding the relevant requirements, though they naturally derive from the topology of the boundaries.

4 Rule-based editing

The exploration of the design space related to the singularities in the pattern is performed through topological modifications of the coarse quad mesh using grammar rules.

4.1 Topological spaces

Indeed, topological spaces are more general than geometrical spaces, which have a metric that allows thorough exploration using continuous-valued design parameters. Nevertheless, topological spaces can be explored using grammars to perform topological transformations in a rule-based design approach. For structural design, original shape grammars evolved into functional grammars (Mitchell (1991)) and then into structural grammars (Mueller (2014)) to include non-geometrical data related to structures. Specific to shell structures, Shea and Cagan (1997) introduce a grammar for the design of structural patterns for geodesic domes, which are triangulated meshes. The grammar required for exploration of singularities is specific for the editing of coarse quad meshes, optionally including pseudo-quads, where most vertices are singular.

4.2 Grammar rules

Infinite combinations exist to modify a set of quads into another. The practical grammar introduced in Figure 11 has been developed based on practice and experience to achieve certain designs with certain goals. This grammar represents a set of tools for the designers and is meant to be further enriched.

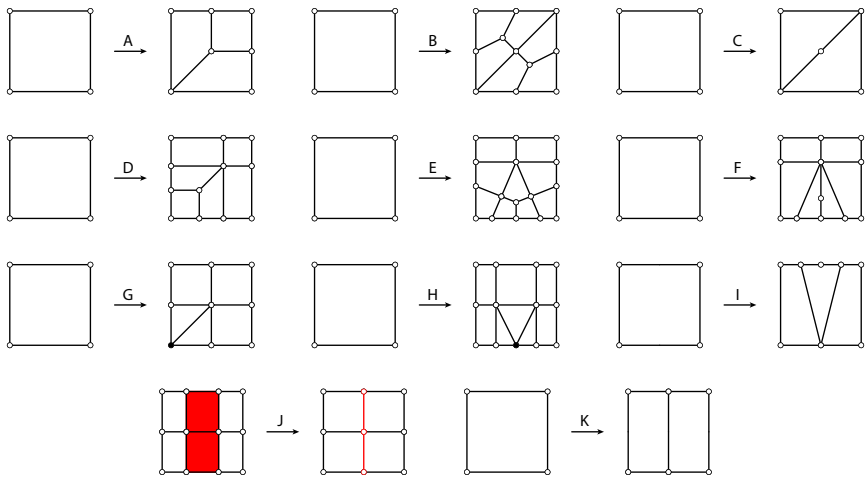

Figure 11: A practical grammar for rule-based editing of coarse quad meshes for singularities in patterns.

Rules A to F split a single quad into multiple quads by adding different sets of singularities, which change the edge flow. Rules G and H add pseudo-quads at a vertex or an edge of a face, respectively. Rule I inserts convex singularities (valency < 3) or concave singularities (valency > 3) at the boundary. Rule J is a coarsening operation which collapses a quad strip (in red), corresponding to one density parameter. Rule K subdivides a quad in two quads without introducing singularities as a utility rule.

After applying one or several of these local rules, a global propagation procedure ensures the validity of the coarse quad mesh. For instance, if a face is modified and one new vertex added on an edge, the adjacent quad face becomes a pentagon, which must be split into two quads, and so on.

4.3 Exploration

A set of designs with different singularities are edited in Figure 12. Starting from the automatically generated topology 0, fifteen other topologies are constructed. The edited coarse quad meshes are projected back onto the input surface. All these designs result from open exploration, without any algorithmic approach, and represent a small set of this unstructured design space.

Topologies 1 to 3 result from coarsening of topology 0 using rule J: topologies 2 and 3 appear as the two simplest ones among the sixteen, with topology 0 as a compromise between them, hence the relevance to start with the medial-axis singularities. Rule K is used for topology 1 to avoid collapsing the opening to only two vertices.
Topologies 4 to 6 result from the applications of rules A to C to the corner quads

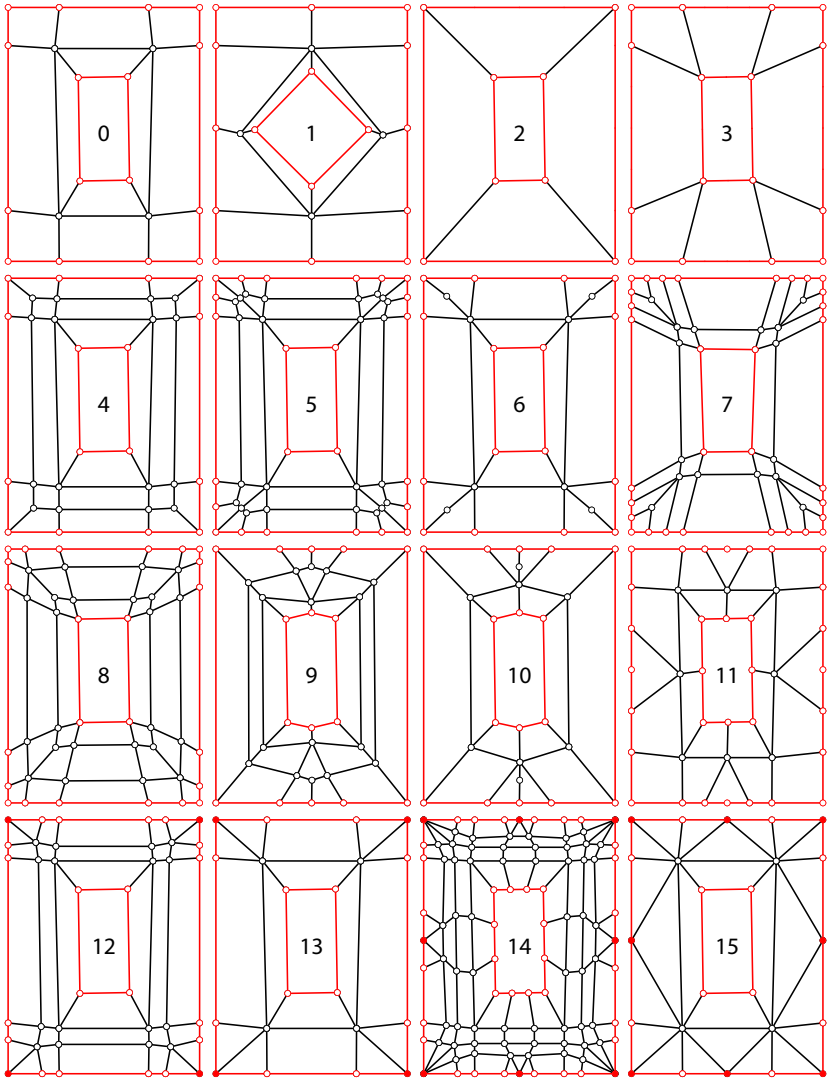

Figure 12: Rule-based exploration of the topological space of singularities in patterns.

of topology 0, respectively. Topologies 7 and 8 result from the applications of rule D to the corner quads of topology 3 with two different orientations.
Topologies 9 and 10 result from the applications of rules E and F to the top and bottom quads of topology 2, respectively. Topology 11 results from the application of rule I to the top, bottom, left and right quads of topology 0.
Topologies 12 and 13 result from the application of rule G to the corner quads of topology 0 to add poles, without and with coarsening using rule J, respectively. Topologies 14 and 15 result from the application of rules J and H to the outer boundary quads of topology 0 to add poles, without and with coarsening using rule J, respectively.

The sequences of applied rules per topology are summarised in Table 1.

Table 1: Sequences of rules applied per topology starting from the automatically generated topology.

topology	rule sequence
0	-
1	K-K-J-J
2	J-J-J-J
3	J
4	A-A-A-A
5	B-B-B-B
6	C-C-C-C
7	D-D-D-D
8	D-D-D-D
9	J-J-J-J-E-E
10	J-J-J-J-F-F
11	I-I-I-I
12	G-G-G-G
13	G-G-G-G-J-J-J-J
14	G-G-G-G-H-H-H-H
15	G-G-G-G-H-H-H-H-J-J-J-J-J-J-J-J

The third challenge is about how to visualise the design space, in spite of the lack of continuous-valued parameters structuring the design space.

5 Performance-driven visualisation

Instead of visualising the design space based on the topology of the pattern, using the performance of each topology for one or several criteria allows to shift the problem to the visualisation of a (potentially high-dimensional) metric space and inform the designer on the relative performance of the different topologies and understand their advantages and drawbacks.

5.1 Designs

All the topologies of the coarse quad meshes in Figure 12 are converted into smooth quad meshes as design patterns shown in Figure 13, which relaxed on the input surface. The density design space formed by the density parameters of the quad strips of the coarse quad mesh is a space in itself which can be subjected to optimisation. Here, the same target length is used to define the density parameters, though it results in differences on the edge length sum, particularly because of poles.

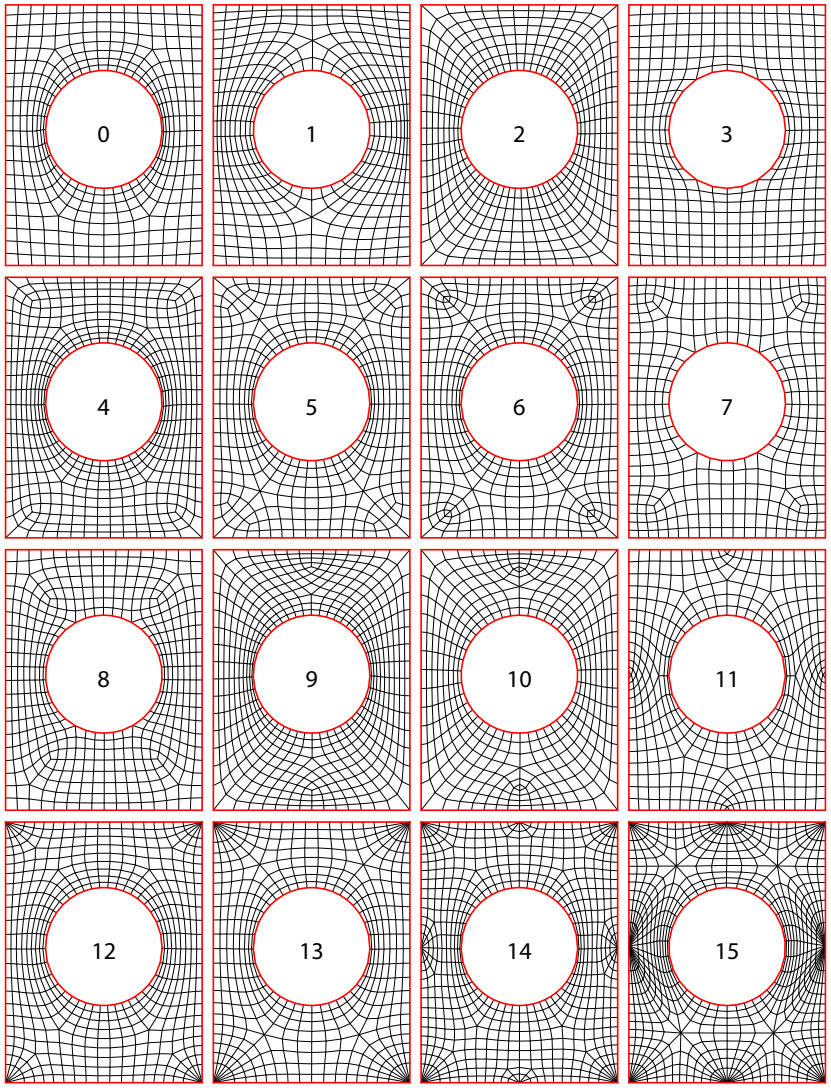

Figure 13: Gridshell pattern designs for the British Museum.

5.2 Performance metrics

The design of a steel and glass gridshell such as the British Museum must integrate a wide range of requirements, among which from fabrication and statics. A few classic of them are considered here.

5.2.1 Fabrication

A first criterion is the planarity of the panels, i.e. the face curvature must be minimised to avoid expensive bending processes. The metric is computed as:

$$C_{mesh} = \frac{1}{A_{mesh}} \sum A_{face} C_{face}, \tag{1}$$

with

$$C_{face} = \frac{dL}{(L_1 + L_2)/2}, \tag{2}$$

where L_1 and L_2 are the lengths of the diagonals of a quad face and dL the shortest distance between them.

A second criterion is the skewness of the panels, i.e. the face skewness must be minimised to reduce material loss when cutting the panels. The metric is computed as:

$$S_{mesh} = \frac{1}{A_{mesh}} \sum A_{face} S_{face}, \tag{3}$$

with

$$S_{face} = \max\left(\frac{\theta_{max} - 90}{90}, \frac{90 - \theta_{min}}{90}\right), \tag{4}$$

where θ_{min} and θ_{max} are the minimal and maximal angles between two consecutive edges in the quad face.

A third criterion is the regularity of the edges, i.e. the variation of edge lengths must be minimised to avoid fabrication of too long or too short elements. The metric is computed as the standard deviation of the edge length in the mesh L_{mesh}.

The optimal parameterisation regarding these fabrication criteria follows the lines of principal curvature (Monge (1798), Liu et al. (2006)). However, the input surface and these lines evolve during geometrical exploration such as form finding and do not relate to structural efficiency.

5.2.2 Statics

Structural efficiency of a pattern depends mainly on the edge flow and its relevance for the considered statics system. Three support conditions shown in Figure 14 are taken into account to highlight this sensitivity: the structure is always vertically supported along its outer and inner boundaries, but thrust is applied either all along its boundaries, at 4 points only (the poles in design 14) or at 8 points only (the poles in design 12). The metrics are computed as the structural mass M_1, M_2 and M_3 after sizing optimisation for each support conditions, respectively.

Some hypothesis are made for comparative analysis.
The S355 steel profiles all have the same tubular cross section and are clamped at the nodes. The tube diameter is minimised for each design with a fixed wall thickness ($t = 40mm$). This choice of unique cross section is meant to favor designs with the most homogeneous stiffness distribution for the considered statics system. The considered load cases are the self-weight G, a vertical downward permanent loading $G' = 1kN/m^2$ and a vertical projected downward snow loading $S = 1kN/m^2$, either on the whole structure (S_0) or on one fourth of the structure (S_1, S_2, S_3, S_4). The SLS and ULS load combinations are $1.0(G+G') + 1.0S_i$ and $1.35(G+G') + 1.5S_i$,

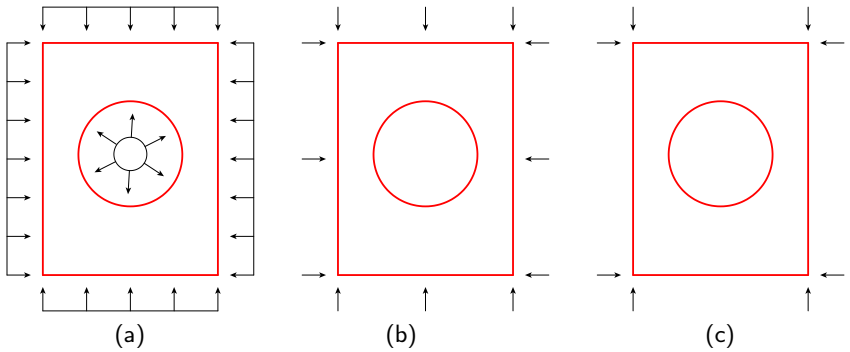

*Figure 14: Considered thrust conditions: (**a**) full boundary thrust for M_1, (**b**) thrust on 8 points for M_2 and (**c**) 4 points only for M_3.*

respectively.

The structural analysis and sizing optimisation are performed in a framework well-known by architects and engineers: Rhino3D and Grasshopper3D using the finite element software Karamba and the gradient-free optimisation library Goat. Constrained optimisation of the structural self-weight is expressed in Equation (5), similarly to Mesnil et al. (2017). Constraints apply on the maximum SLS deflection f_d (60 mm or 1/500^e of the span), the maximum ULS cross-section utilisation ratio u_d (100%) and the minimum ULS buckling load factor p_d (1). Eventually, deflection ends up being the governing constraint, with utilisation ratios staying below 80% and first buckling load factors above 4 for all the designs.

$$\underset{f \leq f_d, u \leq u_d, -p \leq -p_d}{\text{minimize}} \quad M_i \tag{5}$$

5.3 Self-organising maps

The raw results are displayed in Table 2 with the value of each metric for each design and its rank among all the sixteen designs: the lower the metric, the lower the rank and the more efficient the design regarding the metric. As expected, design 14 performs the best for the 8 thrust point support condition thanks to the poles, but more surprisingly, design 7 performs the best for the other support conditions. The mean and the standard deviation are also computed to show the distribution per metric. The metrics M_2 and M_3 featuring different means but similar standard deviations show that the sensitivity to the 8 thrust point support condition is higher than to the one with 4.

The design space can be be visualised based on these results using self-organising maps. Self-organising maps are a neural network technique for dimensionality reduction of a N-dimensional space to a lower dimension. Using the implementation

Table 2: Performance of each design per metric as value and rank.

	C_{mesh} [-]	S_{mesh} [-]	L_{mesh} [-]	M_1 [t]	M_2 [t]	M_3 [t]
0	0,012 (11)	0,091 (2)	0,27 (4)	714 (6)	1818 (15)	2532 (10)
1	0,015 (13)	0,170 (13)	0,30 (9)	864 (15)	1969 (16)	2798 (16)
2	0,009 (7)	0,169 (12)	0,32 (12)	639 (3)	1490 (6)	2448 (7)
3	0,016 (16)	0,082 (1)	0,15 (1)	784 (10)	1755 (14)	2413 (6)
4	0,009 (6)	0,150 (7)	0,27 (5)	758 (7)	1378 (3)	2240 (4)
5	0,007 (4)	0,123 (5)	0,32 (11)	806 (12)	1612 (11)	2534 (11)
6	0,008 (5)	0,167 (11)	0,27 (6)	778 (8)	1379 (4)	2299 (5)
7	0,016 (15)	0,099 (3)	0,20 (2)	610 (1)	1495 (7)	2106 (1)
8	0,016 (14)	0,107 (4)	0,22 (3)	629 (2)	1748 (13)	2552 (13)
9	0,010 (9)	0,188 (14)	0,35 (15)	780 (9)	1561 (9)	2731 (15)
10	0,011 (10)	0,200 (15)	0,33 (13)	656 (4)	1415 (5)	2520 (9)
11	0,014 (12)	0,158 (9)	0,29 (7)	712 (5)	1730 (12)	2544 (12)
12	0,005 (1)	0,146 (6)	0,30 (8)	804 (11)	1531 (8)	2450 (8)
13	0,006 (2)	0,160 (10)	0,33 (14)	816 (14)	1373 (2)	2189 (2)
14	0,007 (3)	0,150 (8)	0,31 (10)	813 (13)	1284 (1)	2225 (3)
15	0,010 (8)	0,310 (16)	0,47 (16)	968 (16)	1579 (10)	2597 (14)
mean	0,011	0,154	0,29	758	1570	2449
st. dev.	0,004	0,053	0,07	95	191	194

by Harding (2016), the initial 6-dimensional performance space is reduced to a 2-dimensional map, as shown in Figure 15.
The performance of each design i is displayed as a bar chart using dimensionless metrics X_i^*:

$$X_i^* = \frac{X_i}{\max_i X_i}. \tag{6}$$

The Voronoi diagram between the designs mark their influence on the underlying map of six-dimensional vectors.

The closer two designs, the more similar their respective performances. Thereof, performance clusters appear: designs 12, 13 and 14 perform well regarding face curvature but badly regarding edge length, because of the poles, and are structurally efficient for thrust at eight or four points; designs 3, 7 and 8 perform well regarding face skewness and edge length but badly regarding face curvature, because of the singularities on the inner boundaries, and are structurally efficient for full thrust; designs 2, 9 and 10 strike a compromise between all the metrics.

This map helps understanding the consequences of a choice of singularities along

the design process and illustrates the necessary trade-off between competing requirements which have to be balanced.

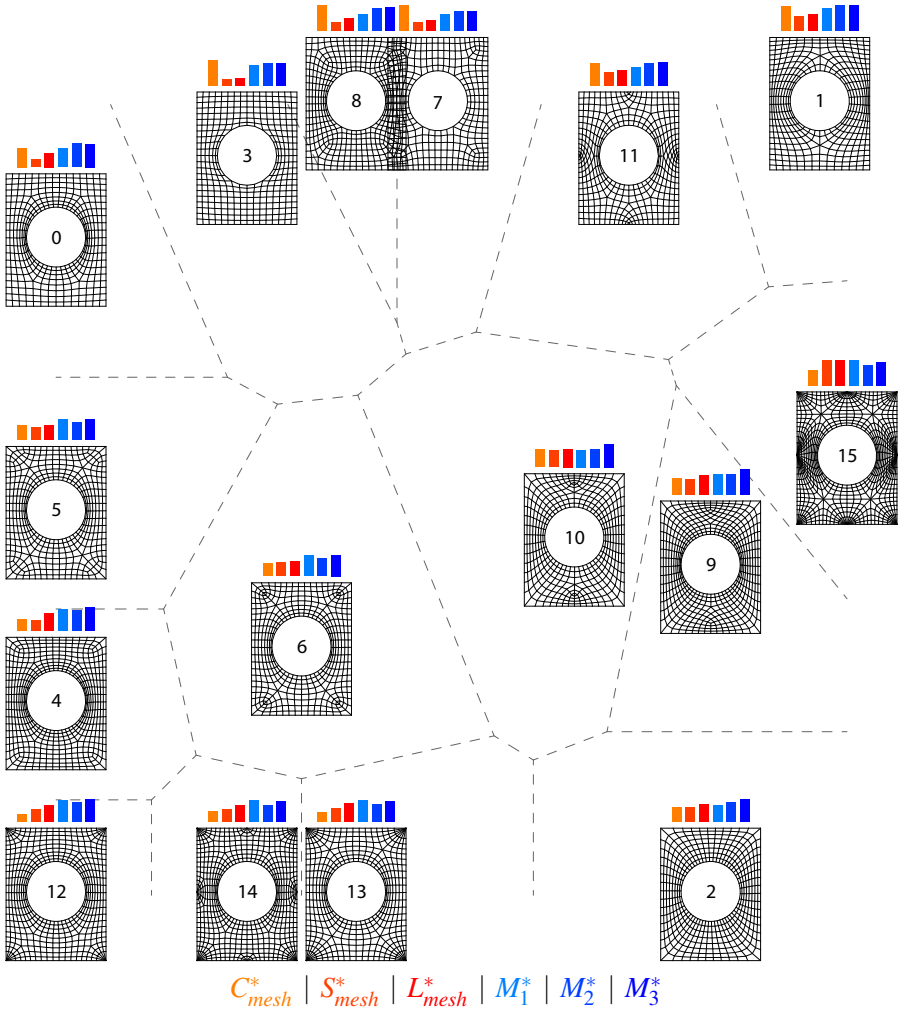

Figure 15: Self-organising map for performance-driven visualisation of the topological design space of singularities.

6 Conclusion

This paper introduces topology finding of structural patterns, complementary to form finding. Design and exploration of the topology of a pattern and its singularities is approached through automated generation and rule-based editing of coarse quad meshes. Design space exploration can be informed via performance-driven visualisation.

Implemented in a practical tool, these design strategies allow the architect and the engineer to explore efficiently the topological design space.

Future work should focus on algorithmic exploration of the design space. A challenge is to shift from performance-informed exploration and resorting to experience and heuristic rules (poles at the location of concentrated forces for structural efficiency, alignment with principal curvature directions for panel planarity...) to guided exploration to well-performing parts of the design space.
Another challenge is the development of automated generation schemes for more general topological shapes. Indeed, the NURBS surfaces here are all disc-homotopic, potentially with perforations, and do not need seams for planar mapping, on the contrary to closed shapes like spheres and non-null genus shapes like tori, which are also part of the topological family of orientable compact manifolds.

References

Blum, H. (1967). A transformation for extracting new descriptors of shape. In *Models for Perception of Speech and Visual Forms*, pp. 362–380. MIT Press.

Botsch, M., L. Kobbelt, M. Pauly, P. Alliez, and B. Lévy (2010). *Polygon mesh processing*. CRC press.

Conway, J. H., H. Burgiel, and C. Goodman-Strauss (2016). *The symmetries of things*. CRC Press.

Harding, J. (2016). Dimensionality reduction for parametric design exploration. In S. Adriaenssens, F. Gramazio, M. Kohler, A. Menges, and M. Pauly (Eds.), *Advances in Architectural Geometry 2016*, pp. 274–87. vdf Hochschulverlag AG.

Harding, J., S. Joyce, P. Shepherd, and C. Williams (2012). Thinking topologically at early stage parametric design. In L. Hesselgren, S. Sharma, J. Wallner, N. Baldassini, P. Bompas, and J. Raynaud (Eds.), *Advances in Architectural Geometry 2012*, pp. 67–76. Springer.

Liu, Y., H. Pottmann, J. Wallner, Y.-L. Yang, and W. Wang (2006). Geometric modeling with conical meshes and developable surfaces. *ACM Transactions on Graphics 25*(3), 681–689.

Mele, T. V., A. Liew, T. Mendéz, M. Rippmann, et al. (2017). COMPAS: A framework for computational research in architecture and structures. http://compas-dev.github.io/compas/.

Mesnil, R., C. Douthe, and O. Baverel (2017). Non-standard patterns for gridshells: fabrication and structural optimization. *Journal of the International Association for Shell and Spatial Structures 58*(4), 277 – 286.

Mitchell, W. J. (1991). Functional grammars: An introduction. In *Proceedings of the Annual Conference of the ACADIA 1991*. CUMINCAD.

Monge, G. (1798). *Géométrie descriptive: leçons données aux écoles normales, l'an 3 de la république*. Baudouin, imprimeur du corps legislatif et de l'institut national.

Mueller, C. T. (2014). *Computational exploration of the structural design space*. Ph. D. thesis, Massachusetts Institute of Technology.

Rigby, D. (2003). Topmaker: A technique for automatic multi-block topology generation using the medial axis. In *ASME/JSME 2003 4th Joint Fluids Summer Engineering Conference*, pp. 1991–1997.

Rippmann, M. and P. Block (2013). Funicular shell design exploration. In *Proceedings of the Annual Conference of the ACADIA 2013*.

Schiftner, A. and J. Balzer (2010). Statics-sensitive layout of planar quadrilateral meshes. In C. Ceccato, P. Hesselgren, M. Pauly, H. Pottmann, and J. Wallner (Eds.), *Advances in Architectural Geometry 2010*, pp. 221–236. Springer.

Shea, K. and J. Cagan (1997). Innovative dome design: Applying geodesic patterns with shape annealing. *Artificial Intelligence for Engineering Design, Analysis and Manufacturing 11*(5), 379–394.

Shepherd, P. and W. Pearson (2013). Topology optimisation of algorithmically generated space frames. In *Proceedings of the International Association for Shell and Spatial Structures Annual Symposium*.

Tang, C., X. Sun, A. Gomes, J. Wallner, and H. Pottmann (2014). Form-finding with polyhedral meshes made simple. *ACM Transactions on Graphics 33*(4), 70:1–70:9.

Williams, C. J. (2001). The analytic and numerical definition of the geometry of the british museum great court roof. In *Mathematics & Design*, pp. 434–440.